Local and Global Gaussian Mixture Models for Hematoxylin and Eosin Stained Histology Image Segmentation

Lei He, L. Rodney Long, Sameer Antani, George R. Thoma

National Library of Medicine, NIH
Bethesda, MD, USA
Lei.He@nih.gov

Abstract—This paper presents a new algorithm for hematoxylin and eosin (H&E) stained histology image segmentation. With both local and global clustering, Gaussian mixture models (GMMs) are applied sequentially to extract tissue constituents such as nuclei, stroma, and connecting contents from background. Specifically, local GMM is firstly applied to detect nuclei by scanning the input image, which is followed by global GMM to separate other tissue constituents from background. Regular RGB (red, green and blue) color space is employed individually for the local and global GMMs to make use of the H&E staining features. Experiments on a set of cervix histology images show the improved performance of the proposed algorithm when compared with traditional K-means clustering and state-of-art multiphase level set methods.

Keywords-Gaussian mixture model; histology; image segmentation; clustering

I. INTRODUCTION

Histology [1, 2, 3] is the study of the microscopic anatomy of cells and tissues of organisms, which is performed by examining a thin slice of tissue under an optical or electron microscope. After a sequential technical procedures (i.e., fixation, dehydration, clearing, infiltration, embedding, sectioning, and staining), histology images can be finally produced by different imaging techniques (e.g. confocal and fluorescence imaging [4]), based on which manual or automated analysis can be conducted to identify abnormal tissues. In present research, the study of histology images is regarded as the gold standard for clinical diagnosis of cancers and identification of prognostic and therapeutic targets. In practice, histopathologists visually examine the regularities of cell shapes and tissue distributions and make corresponding decisions on cancerous regions and malignancy degree. In addition, histology analysis may be applied to connect the tissue study to gene function analysis. For example, in the research of pleiotropy (the association of multiple phenotypes with a single gene), histology analysis provides a potentially powerful tool to study functional genomics by exploring various phenotypic traits.

In current days, manual analysis of digitized histology remains to be the primary instrument to identify cancerous tissues, which depends heavily on the expertise and experiences of histopathologists. Such manual intervention has the disadvantages of time consuming for high-throughput high-content histology images, as well as low repeatability of diagnosis results due to large intra- and inter-operator variations. To overcome these problems, computer assisted

diagnosis (CAD) systems for histology image analysis become increasingly crucial in cancer detection and grading, which always provide instant and consistent results of abnormal region detection. Such computer aided histopathological study has been employed for numerous cancer detection and classification applications, such as prostate [5, 6], breast [7, 8], cervix [9, 10], and lung [12, 13] cancer detection and grading, and neuroblastoma categorization [14], and follicular lymphoma grading [15], just name a few.

A regular CAD system flowchart is shown in Figure 1, which generally consists of procedures of image preprocessing, segmentation, feature extraction and dimension reduction, disease detection and grading, and postprocessing. Note that the order of these modules may be different in practical applications. For example, texture image segmentation requires that texture features should be computed before segmentation. In addition, some modules may be optional in certain applications, which may include other application-specific modules.

For high-content histology images with huge size (e.g. $>10^9$ pixels), image preprocessing can be applied to reduce the computational cost through multi-scale image decomposition such as subsampling [16]. Therefore low resolution images can be analyzed first to roughly locate the regions of interest (ROI), which will be the focus of higher resolution image analysis. In cases of poor image quality with severe noise or blur boundaries, image denoising and enhancement techniques can be applied to increase the image contrast and thus highlight the ROI for an easier segmentation. Traditional image segmentation methods such as edge detection, thresholding, region growing, and K-
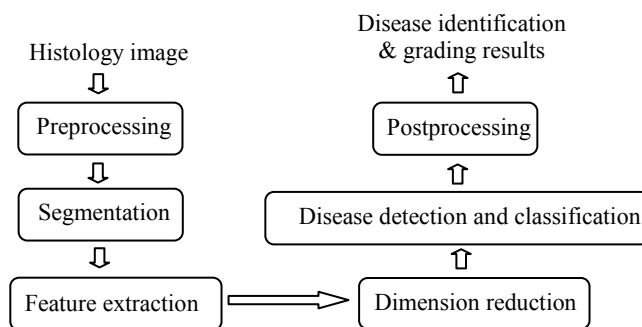

Figure 1. Example of CAD system flowchart for histology image processing and analysis.

means clustering [16, 17] usually require postprocessing (e.g. edge linking or morphological operations) to form continuous and closed boundaries. More advanced segmentation methods include Bayesian models (e.g. Markov random field) [5, 17] and active contours [18]. After image segmentation, a number of features can be extracted from the ROI, including morphometrics [5, 8, 9, 13, 14] with object size and shape (e.g. compactness and regularity), graph-based features [6, 7, 8, 9] (e.g. Voronoi diagram and Delaunay triangulation), intensity and color features (e.g. statistics in different color spaces [5]), and texture features [6, 7, 10, 12, 13, 15] (e.g. Haralick entropy, Gabor filter, power spectrum, co-occurrence matrices, and wavelets). Moreover, besides the regular image domain, many features can also be extracted from other transformed spaces, e.g. frequency (Fourier) space and wavelet transformation [20], which significantly increase the quantity of effective features. Such large number (e.g. >1000) of extracted features are prohibitive for current CAD systems. Thus feature dimension reduction (DR) tools are necessary to find the most discriminative features for practical applications. The commonly used DR tools include both linear (e.g. principal component analysis and linear discriminant analysis) and nonlinear techniques (e.g. spectral clustering and locally linear embedding) [17, 19, 20]. At last, based on the simplified feature vectors, supervised classification algorithms [16, 17] (e.g. support vector machine and neural network) can be applied to identify diseased tissues by comparing the input image features with a set of pre-derived training sample features. In certain applications, postprocessing may be required to derive high level knowledge from the CAD system results. For example, the segmented object shapes may be specifically extracted and stored as indexes for advanced applications like image retrieval. Similarly, image analysis results may be applied for image annotation and information fusion.

In this paper we focus on image segmentation, which is implemented by a two-step algorithm applying both local and global Gaussian mixture models (LG-GMM) to sequentially extract nuclei and other tissue constituents from hematoxylin and eosin (H&E) stained cervix histology images. The paper is organized as follows. After a brief review of image segmentation approaches in Section II, we present our proposed approach in Section III. Section IV shows experimental results, including the comparison with traditional K-Means clustering and state-of-art multiphase level set methods. The paper is summarized in Section V.

II. BACKGROUND

Image segmentation is a fundamental task in current CAD systems. Most existing segmentation methods can be roughly categorized, based on the image features used, into two basic approaches, the edge-based and region-based methods. Early segmentation methods [16, 17] include thresholding, edge detection, region growing, and K-means clustering. Thresholding approaches search for a value (threshold) to separate the objects from the background, typically based on image intensity or its transformation (e.g. Fourier descriptors or wavelets). The threshold is usually

identified to satisfy some constraints or to optimize certain objective functions. For example, the commonly used Otsu's method [16] finds the threshold to maximize the between-class variance. For histology image segmentation, multithresholding approaches [16] are needed to extract different tissue constituents. Edge detection applies spatial filters (e.g. Canny and Sobel filters) to determine the border among objects and background. Region growing [16] groups pixels with similar features (e.g. intensity or texture) into connected areas, each of which is regarded homogenous or smooth according to the predefined feature similarities. K-means clustering groups image points into K clusters by minimizing the objective function as:

$$\sum_{i=1}^{K}\sum_{\mathbf{x}\in S_i}|I_{\mathbf{x}}-\mu_i|^2, \qquad (1)$$

where $I_{\mathbf{x}}$ is the intensity of a point $\mathbf{x}$ in the group S_i, and μ_i is the current mean of S_i.

Typical difficulties in image segmentation include noise, low intensity contrast with weak edges, and intensity inhomogeneity [18], which pose significant challenges to traditional segmentation methods. In addition, traditional approaches like thresholding and edge detection need further operation (e.g. edge linking) to produce continuous object boundaries. To address these difficulties, more recent methods, such as the active contour models, including the key concepts of both the edge-based [21] and region-based approaches [22, 23, 24], have been proposed for image segmentation with promising results. The active contour models can achieve subpixel accuracy and provide closed and smooth contours/surfaces, which become an increasingly important tool for microscopy image segmentation [26, 27].

Edge-based active contours generally use image gradient for object boundary detection, which are sensitive to noise. Therefore region information including intensity, color and texture features has been applied in active contours [22, 23, 24], which usually segment an image into multiple regions of interest with certain homogeneity constraints. In addition, region-based active contours are much less sensitive to contour initialization than edge-based models. For example, the well-known Chan-Vese model (CV) [22] assumes homogeneous object and background regions with distinct intensity means. Given a gray scale image I_0: $\Omega \subset \Re^2 \rightarrow \Re$, the CV energy functional is defined as:

$$E(c_1,c_2,\phi) = \int_{\Omega}(I_0-c_1)^2 H(\phi)d\mathbf{x}$$
$$+ \int_{\Omega}(I_0-c_2)^2(1-H(\phi))d\mathbf{x} + v\int_{\Omega}|\nabla H(\phi)|d\mathbf{x} \qquad (2)$$

where $\mathbf{x}\in\Re^2$ and $v>0$ is a constant. c_1 and c_2 are two global constants representing the intensity means of the two regions, i.e., background and objects. H is the Heaviside step function and ϕ represents the level set function. Eq. (2) handles only gray images with two different regions. To segment H&E stained color histology images with multiple object classes, Eq. (2) has to be extended to multiphase level

sets [23] for vector-valued images, $\mathbf{I}_0: \Omega \subset \Re^2 \rightarrow \Re^3$ [25, 26]. The extended energy functional is:

$$E(\mathbf{c}, \Phi) = \int_\Omega (\mathbf{I}_0 - \mathbf{c}_{11})^2 H(\phi_1) H(\phi_2) d\mathbf{x}$$
$$+ \int_\Omega (\mathbf{I}_0 - \mathbf{c}_{10})^2 H(\phi_1)(1 - H(\phi_2)) d\mathbf{x}$$
$$+ \int_\Omega (\mathbf{I}_0 - \mathbf{c}_{01})^2 (1 - H(\phi_1)) H(\phi_2) d\mathbf{x} \quad (3)$$
$$+ \int_\Omega (\mathbf{I}_0 - \mathbf{c}_{00})^2 (1 - H(\phi_1))(1 - H(\phi_2)) d\mathbf{x}$$
$$+ v \int_\Omega |\nabla H(\phi_1)| d\mathbf{x} + v \int_\Omega |\nabla H(\phi_2)| d\mathbf{x}$$

where $\mathbf{c} = (\mathbf{c}_{00}, \mathbf{c}_{01}, \mathbf{c}_{10}, \mathbf{c}_{11})$ represents the average vector (RGB) values of four image regions produced by two level sets $\Phi = (\phi_1, \phi_2)$. By calculus of variations, the level set evolution equation can be derived as:

$$\frac{\partial \phi_1}{\partial t} = \delta(\phi_1)\{v \, \mathrm{div}(\frac{\nabla \phi_1}{|\nabla \phi_1|}) - ((\mathbf{I}_0 - \mathbf{c}_{11})^2 - (\mathbf{I}_0 - \mathbf{c}_{01})^2) H(\phi_2)$$
$$- ((\mathbf{I}_0 - \mathbf{c}_{10})^2 - (\mathbf{I}_0 - \mathbf{c}_{00})^2)(1 - H(\phi_2))\}$$
$$\quad (4)$$
$$\frac{\partial \phi_2}{\partial t} = \delta(\phi_2)\{v \, \mathrm{div}(\frac{\nabla \phi_2}{|\nabla \phi_2|}) - ((\mathbf{I}_0 - \mathbf{c}_{11})^2 - (\mathbf{I}_0 - \mathbf{c}_{10})^2) H(\phi_1)$$
$$- ((\mathbf{I}_0 - \mathbf{c}_{01})^2 - (\mathbf{I}_0 - \mathbf{c}_{00})^2)(1 - H(\phi_1))\}$$

δ is the Dirac function.

With a different framework to extract multiple objects, Samson's image classification model [24] applies a group of level sets, $(\phi_1, \ldots, \phi_K)$, to divide the input image into K regions, each of which corresponds to the interior of a level set, i.e., $\phi_i > 0$.

$$E(\phi_1, \ldots, \phi_K) = \sum_{i=1}^K e_i \int_\Omega H(\phi_i) \frac{(I_0 - \mu_i)^2}{\sigma_i^2} d\mathbf{x}$$
$$\quad (5)$$
$$+ \sum_{i=1}^K \gamma_i \int_\Omega g(I_0)\delta(\phi_i)|\nabla \phi_i| d\mathbf{x} + \frac{\lambda}{2}\int_\Omega (\sum_{i=1}^K H(\phi_i) - 1)^2 d\mathbf{x}$$

where $e_i > 0$, $\gamma_i > 0$, and $\lambda > 0$ are constants to balance the terms. $g(I_0) = \frac{1}{1 + |\nabla G_\sigma * I_0|^2}$ is a monotonically decreasing function, which deforms contours towards edges. Briefly, the first term in Eq. (5) ensure a homogeneous region within each level set, which can be fitted by a Gaussian distribution with pre-estimated mean μ_i and variance σ_i^2. The second term prefers a smooth curve at edges, and the third term prevents overlapping level sets. The level set evolution equations are:

$$\frac{\partial \phi_i}{\partial t} = -\delta(\phi_i)\{e_i \frac{(I_0 - \mu_i)^2}{\sigma_i^2} - \gamma_i g(I_0) div(\frac{\nabla \phi_i}{|\nabla \phi_i|})$$
$$\quad (6)$$
$$- \frac{\nabla g \nabla \phi_i}{|\nabla \phi_i|} + \lambda(\sum_{i=1}^K H(\phi_i) - 1)\}$$

In this paper we compare our LG-GMM algorithm with traditional K-means clustering and the advanced region-based level set methods, i.e., the extended CV model (Eq. (4)) and Samson's model (Eq. (6)).

III. PROPOSED APPROACH

A. Gaussian Mixture Model

Mixture models [11] are widely used to approximate complicated distributions with the output coming from one of a group of "hidden" sources (e.g. objects and background in an image), which provides a general framework to characterize heterogeneity. In this paper, we choose mixture models for our specific application of histology image segmentation, which consists of multiple classes of objects widely distributed in the image. In statistics, a mixture model is usually defined as a probability distribution that is a convex combination of several independent components with different probability distributions. Given an output, the goal is to estimate from which source (measured by probabilities) the output is generated, as well as the parameters describing the source component distributions, e.g. means and variances of a GMM. With a set of N samples (image points) from n-dimensional space, $X = \{\mathbf{x}_1, \ldots, \mathbf{x}_j, \ldots, \mathbf{x}_N\}$, in which each sample is drawn from one of M Gaussian components, a GMM can be denoted as:

$$p(X | \Theta) = \sum_{i=1}^M \alpha_i p_i(X | \theta_i), \quad (7)$$

where the parameters are $\Theta = \{\alpha_1, \ldots, \alpha_M, \theta_1, \ldots, \theta_M\}$ such that $\sum_{i=1}^M \alpha_i = 1$ and α_i refers to the prior probability of each component; $\theta_i = (\mu_i, \Sigma_i)$, μ_i is the mean and Σ_i is the covariance matrix, $i=1, \ldots M$. Let $y_j, j=1, \ldots N$, denote which Gaussian $\mathbf{x}_j$ is drawn from, the probability of $\mathbf{x}_j$ coming from the i-th Gaussian is:

$$P(\mathbf{x}_j | y_j = i, \theta_i) = \frac{\exp\left(-\frac{1}{2}(\mathbf{x}_j - \mu_i)^T \Sigma_i^{-1}(\mathbf{x}_j - \mu_i)\right)}{(2\pi)^{n/2} |\Sigma_i|^{1/2}}, \quad (8)$$

The task is to estimate the hidden distributions given the data, i.e., to estimate the unknown parameters Θ which maximize Eq. (8). The GMM parameters can be estimated by the expectation-maximization (EM) algorithm [28], which repeats the E-step and M-step until convergence. The E-step is to calculate the expectation of which Gaussian is used, conditioned on the observations (X), using the estimated prior probability of each distribution ($p(y_j = i | \theta_i)$) and current parameter values (Θ_t),

$$p(y_j = i | \mathbf{x}_j, \Theta_t) = \frac{p(\mathbf{x}_j | y_j = i, \Theta_t) p(y_j = i | \Theta_t)}{\sum_{k=1}^M p(\mathbf{x}_j | y_j = k, \Theta_t) p(y_j = k | \Theta_t)} \quad (9)$$

Given the E-step estimation of unknown variables ($\mathbf{y}$ = $\{y_1,\ldots,y_N\}$, y_j=1,…,M), the M-step estimates the distribution parameters (Θ) and the prior probability of each distribution, which maximize the data likelihood as

$$Q(\Theta,\Theta_t) = E_y\left[\log \prod_{j=1}^{N} p(\mathbf{x}_j,\mathbf{y}\,|\,\Theta)\Big|\mathbf{x}_j\right] \quad (10)$$

$$= \sum_{j=1}^{N}\sum_{i=1}^{M} p(y_j = i\,|\,\mathbf{x}_j,\Theta_t)\log(p(\mathbf{x}_j\,|\,y_j = i,\Theta)p(y_j = i\,|\,\Theta))$$

where the log-likelihood is used for easier numerical implementation. With gradient ascent approach, we can update the parameters and the prior probabilities as:

$$\mu_i = \frac{\sum_{j=1}^{N} p(y_j = i\,|\,\mathbf{x}_j,\Theta_t)\mathbf{x}_j}{\sum_{j=1}^{N} p(y_j = i\,|\,\mathbf{x}_j,\Theta_t)} \quad (11)$$

$$\Sigma_i = \frac{\sum_{j=1}^{N} p(y_j = i\,|\,\mathbf{x}_j,\Theta_t)(\mathbf{x}_j - \mu_i)(\mathbf{x}_j - \mu_i)^T}{\sum_{j=1}^{N} p(y_j = i\,|\,\mathbf{x}_j,\Theta_t)}$$
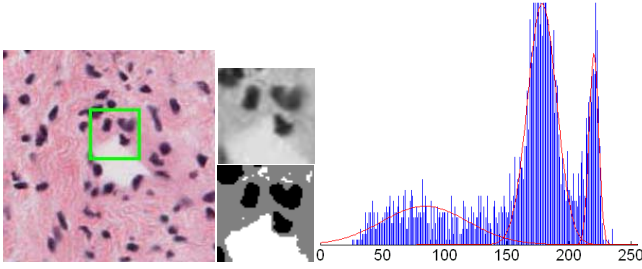

Figure 2. Local GMM distribution estimation example.

These updated parameters then become the input for next E-step, and the convergence to a local maximum of the EM algorithm is guaranteed [28]. Using the EM algorithm, Figure 2 shows an example of local GMM-based distribution estimation in a small region (see the green rectangle). The left image in Figure 2 is an input image with three target classes of nuclei, connecting tissue constituents, and background, which is cropped (size 200×200) from a large size cervix histology image (size 72360×41788). The middle top image is the gray scale version of the selected region. The middle bottom image is the segmentation result based on the estimated distribution, i.e., each pixel is grouped to the cluster (distribution) to which it has the closest distance. The blue lines in the right image correspond to the intensity histogram of the region. The estimated Gaussian distributions of the objects and background are illustrated as the red curves. It can be seen that the estimated distributions match well with the real intensity histogram, which show the suitability to use the GMM for objects and background distribution estimation.

B. LG-GMM Segmentaiton Algorithm

The proposed LG-GMM segmentation algorithm employs the unique characteristics of the H&E staining protocol: hematoxylin stains nuclei blue; eosin stains the cytoplasm pink, red blood cells red; air spaces are white. Therefore, we can obtain that nuclei are always represented by dark points, see Figure 2 example. In addition, other tissue connecting constituents all have high R values like those in background, which can be well separated with their G or B values. Based on these observations, we derive our two-step algorithm as: (1) nuclei detection by local GMMs; (2) other tissue constituents extraction by a global GMM.

In the first step, local GMMs are employed to extract nuclei by scanning the R channel of the input image with a window. Specifically, for each image region under the scanning window, the local intensity distribution is estimated by a local GMM with a prior number of different target classes in the image, e.g. 3 for Figure 2 example. In practice, the number of classes falling into the scanning window may be different from the total number in the whole image. Our algorithm is robust to such variation because we focus on only the dark points in each scanning window. After the intensity (R) distribution estimation in a region, each pixel with the closest distance to the darkest class is labeled as a nucleus point. Figure 3(a) shows the detected nuclei from the left image in Figure 2 after the first step.
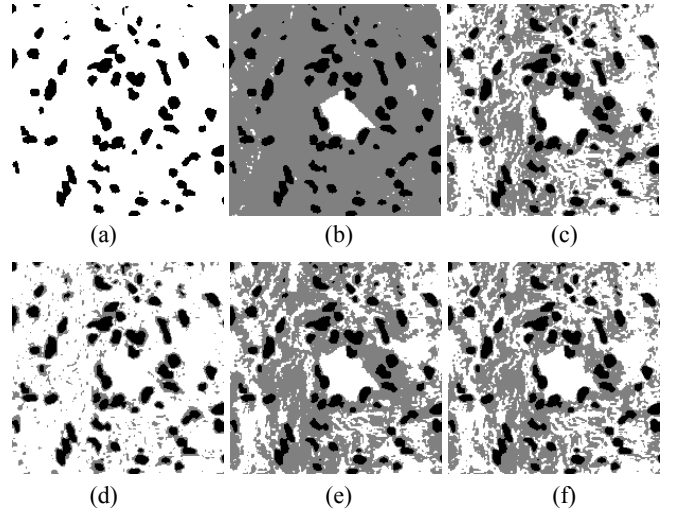

Figure 3. LG-GMM segmentation example: (a) nuclei dection. (b) segmentation result on the RGB space. (c) segmentation result on gray scale image. (d), (e), (f) segmentation result on the R, G, and B channels.

In the second step, a global GMM is applied to either G or B channel to group the rest of image points into different clusters, which again makes use of the H&E staining features. Together with the first step result, Figure 3(b) shows the final segmentation result of Figure 2 example, with black pixels representing nuclei, gray pixels for stroma and other tissue constituents connecting cells, and white pixels for background. To show the advantages of exploiting the H&E staining features, we also apply the same algorithm to the gray scale image, and the R, G, and B channels

respectively, see Figures 3(c)-(f). It can be seen that with the specific prior knowledge of H&E staining features, our algorithm obtains rather encouraging result.

IV. EXPERIMENTS

In this section, in addition to the example in Figure 2, three more images cropped from H&E stained cervix histology images are used to illustrate the superior performance of the proposed algorithm when compared with both traditional K-means clustering and current advanced multiphase level set methods [22, 23, 24]. K-means and Samson's model implement segmentation on gray scale images. Multiple uniformly distributed seeds are used as the initial level sets for all the examples in our experiments. For an efficient computational cost, in our experiments we choose the scanning window size to be a quarter of the input image. Figure 4 shows the results of K-means clustering (left), CV multiphase model (middle) and Samson's model (right). With rather close intensities between the connecting tissue constituents and the background, these methods cannot accurately differentiate them.
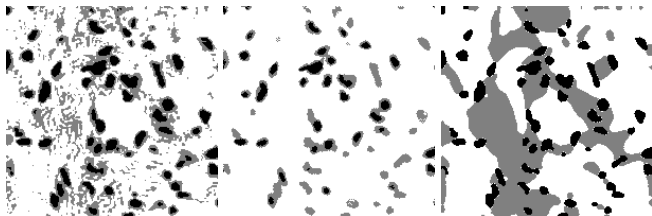

Figure 4. Image segmentation result of K-means (left), CV model (middle), and Samson's model (right).

Figure 5 demonstrates three examples with different numbers of target classes. The left image (size 500×350) consists of three classes: nuclei, connecting tissue constituents in epithelium, in addition to background. The other two images (size 400×400) include four target classes: nuclei, red blood cells (stroma), connecting tissue constituents, and background. The left image is similar to Figure 2 example with some blurry nuclei embedded in the epithelium, and the difficulty lies in the fine texture structure at the left side. The other two images are rather challenging with complicated object distributions. Specifically, in the second image, the blood cells in the middle part are rather similar to the connecting tissue constituents at the bottom left region. In the right image, the boundary between the left stroma and the right epithelium is mixed with all different target classes. The input images, the results of our LG-GMM (row 2), K-means clustering (row 3), CV multiphase level set model (row 4), and Samson's model (row 5) are listed from the top to bottom. Again, we can see that our proposed LG-GMM algorithm outperforms other approaches for all the three images. For the simple example of the left image, all methods can obtain good results. Though, minor texture details are missed by Samson's level set method, as shown by the red rectangle. For the middle image, our method successfully extracts the blood cells (dark gray regions as shown by the arrow in row 2) from the surrounding tissue

constituents (light gray regions). Similarly, for the right image, the stroma (left dark gray regions) and the epithelium (right light gray regions) are well separated by the proposed LG-GMM algorithm. The other three methods fail to produce accurate results for these two difficult examples. The main reason is because only the global region homogeneity is used to constrain the segmentation, which cannot differentiate minor intensity differences in local regions well, especially for inhomogeneous histology images with widely distributed objects. In this case, local contrast information is needed for accurate segmentation, as in our proposed LG-GMM algorithm.
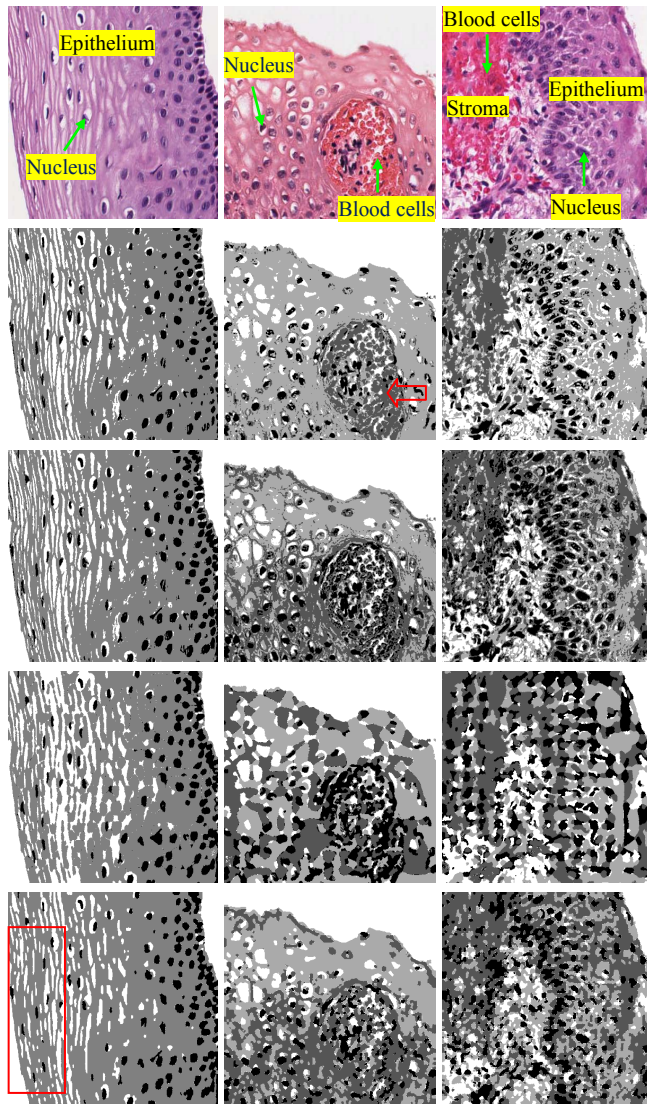

Figure 5. Original images (row 1) and segmentation results of our method (row 2), K-means (row 3), CV (row 4), and Samson's model (row 5).

V. SUMMARY

This paper presents a new algorithm for robust H&E stained histology image segmentation. Local and global Gaussian mixture models are applied sequentially in

different color channels to extract nuclei and other tissue constituents. Compared with traditional K-means clustering, and state-of-art multiphase level set methods, our model provides a rather simple and flexible framework to solve such challenging segmentation problem. In addition, with the only parameters of scanning window size and number of target classes, the proposed algorithm obtains more robust and accurate results than existing approaches. Based on the segmentation results, future work including feature extraction in the ROI and classification are planned for cancer detection and malignancy level grading, e.g. cervical intraepithelial neoplasia grading with cervix histology images or Gleason grading for prostate histology images.

REFERENCES

[1] L. P. Gartner and J. L. Hiatt, Color Textbook of Histology: with Student Consult Online Access. Saunders, 3rd ed., 2006.

[2] J. A. Kiernan, Histological and Histochemical Methods: Theory and Practice. Cold Spring Harbor Laboratory Press, 4th ed., 2008.

[3] S. E. Mills, Histology for Pathologists. Lippincott Williams & Wilkins, 3rd ed., 2006.

[4] D. B. Murphy, Fundamentals of Light Microscopy and Electronic Imaging. Wiley-Liss, 2001.

[5] J. Monaco, J. Tomaszewski, M. Feldman, M. Mehdi, P. Mousavi, A. Boag, C. Davidson, P. Abolmaesumi, and A. Madabhushi, "Probabilistic Pair-wise Markov Models: Application to Prostate Cancer Detection," Proc. SPIE Medical Imaging, SPIE Press, 2009, vol.7260, doi:10.1117/12.812462.

[6] S. Doyle, M. Hwang, K. Shah, A. Madabhushi, J. Tomasezweski, and M. Feldman, "Automated Grading of Prostate Cancer Using Architectural and Textural Image Features," Proc. IEEE International Symposium on Biomedical Imaging (ISBI 07), IEEE Press, 2007, pp. 1284-1287, doi:10.1109/ISBI.2007.357094.

[7] S. Doyle, S. Agner, A. Madabhushi, M. Feldman, and J. Tomaszewski, "Automated Grading of Breast Cancer Histopathology Using Spectral Clustering with Textural and Architectural Image Features," Proc. IEEE International Symposium on Biomedical Imaging (ISBI 08), IEEE Press, 2008, pp. 496-499, doi:10.1109/ISBI.2008.4541041.

[8] S. Naik, S. Doyle, S. Agner, A. Madabhushi, M. Feldman, and J. Tomaszewski, "Automated Gland and Nuclei Segmentation for Grading of Prostate and Breast Cancer Histopathology," Proc. IEEE International Symposium on Biomedical Imaging (ISBI 08), IEEE Press, 2008, pp. 284-287, doi:10.1109/ISBI.2008.4540988.

[9] S. J. Keenan, J. Diamond, W. G. McCluggage, H. Bharucha, D. Thompson, P. H. Bartels, and P. W. Hamilton, "An Automated Machine Vision System for The Histological Grading of Cervical Intraepithelial Neoplasia (CIN)," Journal of Pathology, vol. 192, Aug. 2000, pp. 351-362, doi:10.1002/1096-9896(2000)9999:9999<::AID-PATH708>3.0.CO;2-I.

[10] M. Guillauda, K. Adler-Storthz, A. Malpica, G. Staerkel, J. Matisic, D. V. Niekirkd, D. Cox, N. Poulina, M. Follen, and C. MacAulaya, "Subvisual Chromatin Changes in Cervical Epithelium Measured by Texture Image Analysis and Correlated with HPV," Gynecologic Oncology, vol. 99, Dec. 2005, pp. S16-S23, doi:10.1016/j.ygyno.2005.07.037.

[11] G. J. McLachlan and D. Peel, Finite Mixture Models. Wiley, 2000.

[12] K. Schmid, N. Angerstein, S. Geleff, and A. Gschwendtner, "Quantitative Nuclear Texture Features Analysis Confirms WHO Classification 2004 for Lung Carcinomas," Modern Pathology, vol. 19, Feb. 2006, pp. 453-459, doi:10.1038/modpathol.3800541.

[13] U. Jütting, P. Gais, K. Rodenacker, J. Böhm, S. Koch, H. W. Präuer, and H. Höfler, "Diagnosis and Prognosis of Neuroendocrine Tumors of The Lung by Means of High Resolution Image Analysis," Analytical Cell Pathology, vol. 18, Jan. 1999, pp. 109-119.

[14] J. Kong, O. Sertel, H. Shimada, K. L. Boyer, J. H. Saltz, and M. N. Gurcan, "Computer-aided Evaluation of Neuroblastoma on Whole-slide Histology Images: Classifying Grade of Neuroblastic Differentiation," Pattern Recognition, vol. 42, Jun. 2009, pp. 1080-1092, doi:10.1016/j.patcog.2008.10.035.

[15] O. Sertel, J. Kong, G. Lozanski, U. Catalyurek, J. Saltz, and M. N. Gurcan, "Computerized microscopic image analysis of follicular lymphoma," Proc. SPIE Medical Imaging, 2008, vol. 6915, doi:10.1117/12.770936.

[16] R. C. Gonzalez and R. E. Woods, Digital Image Processing. Pearson Prentical Hall, 3rd ed., 2008.

[17] C. M. Bishop, Pattern Recognition and Machine Learning. Springer, 2006.

[18] L. He, Z. Peng, B. Everding, X. Wang, C. Han, K. Weiss, and W. G. Wee, "A Comparative Study of Deformable Contour Method in Medical Image Segmentation," Image and Vision Computing, vol. 26, Feb. 2008, pp. 141-163, doi:10.1016/j.imavis.2007.07.010.

[19] G. Lee, C. Rodriguez, and A. Madabhushi, "Investigating The Efficacy of Nonlinear Dimensionality Reduction Schemes in Classifying Gene- and Protein-Expression Studies," IEEE/ACM Trans. on Computational Biology and Bioinformatics, vol. 5, Jul. 2008, pp. 368-384, doi:10.1109/TCBB.2008.36.

[20] N. Orlov, J. Johnston, T. Macura, L. Shamir, and I. Goldberg, "Computer vision for microscopy applications," in Vision Systems – Segmentation and Pattern Recognition, G. Obinata and A. V. Dutta, Eds. ARS Press, 2007, pp. 221-242.

[21] V. Caselles, R. Kimmel, and G. Sapiro, "Geodesic Active Contours," International Journal of Computer Vision, vol. 22, Feb. 1997, pp. 61-79, doi:10.1023/A:1007979827043.

[22] T. F. Chan and L. A. Vese, "Active Contour Without Edges," IEEE Trans. on Image Processing, vol. 10, Feb. 2001, pp. 266-277, doi:10.1109/83.902291.

[23] L. A. Vese and T. F. Chan, "A Multiphase Level Set Framework for Image Segmentation Using the Mumford and Shah Model," International Journal of Computer Vision, vol. 50, Dec. 2002, pp. 271-293, doi:10.1023/A:1020874308076.

[24] C. Samson, L. Blanc-Féraud, G. Aubert, and J. Zerubia, "A Level Set Model for Image Classification," International Journal of Computer Vision, vol. 40, Dec. 2000, pp. 187-197, doi: 10.1023/A:1008183109594.

[25] T. F. Chan, B. Sandberg, and L. A. Vese, "Active Contours Without Edges for Vector-valued Images," Journal of Visual Communication and Image Representation, vol. 11, Jun. 2000, pp. 130-141, doi:10.1006/jvci.1999.0442.

[26] A. Hafiane, F. Bunyak, and K. Palaniappan, "Level Set-based Histology Image Segmentation with Region-based Comparison," Proc. Microscopic Image Analysis with Applications in Biology (MIAAB 08), 2008.

[27] J. Degerman, J. Faijerson, K. Althoff, T. Thorlin, J. H. Rodriguez, and T. Gustavsson, "A Comparative Study Between Level Set and Watershed Image Segmentation for Tracking Stem Cells in Time-lapse Microscopy," Proc. Microscopic Image Analysis with Applications in Biology (MIAAB 06), 2006.

[28] A. Dempster, N. Laird, and D. Rubin, "Maximum Likelihood From Incomplete Data Via the EM Algorithm," Journal of the Royal Statistical Society - Series B, vol. 39, 1977, pp. 1-38.